Published in final edited form as:
Nat Cell Biol. 2008 November ; 10(11): 1309. doi:10.1038/ncb1789.

IAPs contain an evolutionarily conserved ubiquitin-binding domain that regulates NF-κB as well as cell survival and oncogenesis

Mads Gyrd-Hansen[1,2,10,11], **Maurice Darding**[1,10], **Maria Miasari**[3], **Massimo M. Santoro**[4,5], **Lars Zender**[6], **Wen Xue**[6,7], **Tencho Tenev**[1], **Paula C.A. da Fonseca**[8], **Marketa Zvelebil**[1], **Janusz M. Bujnicki**[9], **Scott Lowe**[6], **John Silke**[3], and **Pascal Meier**[1,11]

[1] Breakthrough Toby Robins Breast Cancer Research Centre, Institute of Cancer Research, Mary-Jean Mitchell Green Building, Chester Beatty Laboratories, Fulham Road, London SW3 6JB, UK [3] Department of Biochemistry, Level 4 RL Reid Building, La Trobe University, Victoria 3086, Australia [4] Molecular Biotechnology Center, University of Torino, Torino 10126, Italy [5] Department of Environmental and Life Sciences, University of Piemonte Orientale, Alessandria 15100, Italy [6] Cold Spring Harbor Laboratory, NY-11724, USA [7] Helmholtz Centre for Infection Research, Braunschweig 38124, Germany and Department. of Gastroenterology, Hepatology and Endocrinology, Hannover Medical School, Hannover 30625, Germany [8] Section of Structural Biology, The Institute of Cancer Research, Chester Beatty Laboratories, Fulham Road, London SW3 6JB, UK [9] International Institute of Molecular and Cell Biology in Warsaw, ul. Trojdena 4, 02-109 Warsaw, and Adam Mickiewicz University, ul. Umultowska 89, 61-614 Poznan, Poland

Abstract

The covalent attachment of ubiquitin to target proteins influences various cellular processes, including DNA repair, NF-κB signalling and cell survival1. The most common mode of regulation by ubiquitin-conjugation involves specialized ubiquitin-binding proteins that bind to ubiquitylated proteins and link them to downstream biochemical processes. Unravelling how the ubiquitin-message is recognized is essential because aberrant ubiquitin-mediated signalling contributes to tumour formation2. Recent evidence indicates that inhibitor of apoptosis (IAP) proteins are frequently overexpressed in cancer and their expression level is implicated in contributing to tumorigenesis, chemoresistance, disease progression and poor patient-survival[3]. Here, we have identified an evolutionarily conserved ubiquitin-associated (UBA) domain in IAPs, which enables them to bind to Lys 63-linked polyubiquitin. We found that the UBA domain is essential for the oncogenic potential of cIAP1, to maintain endothelial cell survival and to protect cells from TNF-α-induced

11Correspondence should be addressed to P.M. or M.G.-H. (pmeier@icr.ac.uk; mads.gyrd@bric.dk).
[2]Current address: Biotech Research and Innovation Centre, University of Copenhagen, Ole Maaloees Vej 5, DK-2200 Copenhagen, Denmark.
[10]These authors contributed equally to this work.

Note: Supplementary Information is available on the Nature Cell Biology website.

COMPETING FINANCIAL INTERESTS
The authors declare no competing financial interests.

AUTHOR CONTRIBUTIONS
M.G.-H. and M.D. performed all experiments, except for those in Fig. 4; M.M. and J.S. planned and performed the cIAP1$^{-/-}$ MEF reconstitution assay; M.M.S. planned and performed the zebrafish reconstitution assay; L.Z., W.X. and S.L. designed, performed and supervised the cIAP1 mouse tumour assay; T.T. provided various constructs and technical support; P.C.A.F. performed sequence alignments and database searches with structural prediction algorithms; J.M.B and M.Z. performed 3D modelling and sequence analysis; M.G.-H. and P.M. designed and supervised the study and wrote the paper.

apoptosis. Moreover, the UBA domain is required for XIAP and cIAP2–MALT1 to activate NF-κB. Our data suggest that the UBA domain of cIAP2–MALT1 stimulates NF-κB signalling by binding to polyubiquitylated NEMO. Significantly, 98% of all cIAP2–MALT1 fusion proteins retain the UBA domain, suggesting that ubiquitin-binding contributes to the oncogenic potential of cIAP2–MALT1 in MALT lymphoma. Our data identify IAPs as ubiquitin-binding proteins that contribute to ubiquitin-mediated cell survival, NF-κB signalling and oncogenesis.

The conjugation of ubiquitin (Ub) to target proteins plays an important part in the formation of signalling networks. The Ub modification is recognized through low-affinity, non-covalent interactions between Ub and small Ub-binding domains present in specialized proteins that are collectively referred to as Ub-receptors. These receptors are responsible for translating Ub modifications into cellular phenotypes. Ub can be attached to target proteins as a single moiety (monoubiquitylation), or as polyUb chains. For polyubiquitylation, the Ub molecules are generally linked through Lys 48 and Lys 63 of Ub. Lys 48-linked polyUb chains adopt a kinked topology, whereas those of Lys 63 are more linear and resemble 'beads-on-a-string'[4,5]. Ub-receptors that recognize Lys 48-linked polyUb chains recruit the modified proteins to the proteasome for degradation. In contrast, Ub-receptors that bind to monoUb or Lys 63 linkages enable non-degradative signalling processes by recruiting monoUb or Lys 63-polyubiquitylated proteins to downstream protein complexes2. Lys 63-linked ubiquitylation, for example, is used as a key signal transducer for activation of NF-κB and cell survival.

IAPs are characterized by the presence of the baculovirus IAP repeat (BIR) domain[6]. In addition, some IAPs, such as XIAP, cIAP1 and cIAP2, also contain a RING finger that provides them with Ub ligase (E3) activity. Although best known for their ability to regulate caspases and apoptosis, IAPs also influence signalling pathways that lead to activation of the NF-κB pathway7−13. For example, recent evidence indicates that cIAP1 is required to modulate NF-κB activation and suppress TNF-α-mediated apoptosis7−9,13,14. Further, reciprocal translocation of cIAP2 and MALT1 generates a cIAP2–MALT1 fusion protein that drives constitutive NF-κB activation and B-cell transformation[11,15]. Currently, little is known about how IAPs contribute to NF-κB regulation, cell survival and tumour growth.

Using sequence analysis and structural prediction algorithms, we noticed a previously unrecognized, evolutionarily conserved UBA domain within the linker region between the third BIR domain and the RING finger of IAPs such as cIAP1, cIAP2 and XIAP-like proteins (Fig. 1a; Supplementary Information, Fig. S1). The motif is present exclusively in IAPs with three BIR domains and a RING finger, with the exception of ILP-2/BIRC8. The UBA domain is a short protein fold that consists of three tightly packed α-helices (Supplementary Information, Fig. S1), which mediate Ub-binding. The UBA domain enables host proteins to participate in Ub-dependent signalling processes[16]. Structural studies indicate that a conserved hydrophobic patch on the UBA domain makes direct contact with Ub. This patch is composed of residues positioned immediately C-terminal to the α1 helix ('MGF' motif) and two aliphatic residues at the end of the α3 helix ('LL/V' motif, Fig. 1b; Supplementary Information, Fig. S1)[17,18]. Importantly, the three-helix bundle and the MGF, as well as LL/V motifs, are also present in the putative UBA of IAPs (Fig. 1b; Supplementary Information, Fig. S1b). Moreover, the predicted tertiary structures of the IAP UBA are very similar to those of known UBA-domain-containing proteins (Supplementary Information, Fig. S1c and data not shown).

Different types of UBA domains show distinct monoUb and linkage-selective polyUb-binding ability[19]. To examine the Ub-binding properties of IAPs, we assessed whether recombinant cIAP1, cIAP2, XIAP and DIAP2 associate with monoUb, Lys 63- and Lys 48-linked polyUb chains. None of the IAPs interacted with monoUb but they bound efficiently to Lys 63-linked polyUb, and in some cases to Lys 48-linked polyUb chains (Fig. 1c–l). cIAP1 and DIAP2 seemed to bind both Lys 63- and Lys 48-linked polyUb similarly, whereas cIAP2 and XIAP

were highly specific for Lys 63 conjugates. Binding to Lys 63- and Lys 48-linked polyUb chains was UBA-domain-dependent because point mutations in the conserved MGF motif or deletion of this domain, abrogated the interaction. Although DIAP2 carries LGI and IF residues at the corresponding positions of the classical MGF and LL/V motif of other UBA domains, these changes preserve the hydrophobic surface required for Ub binding. Consistent with this, mutations in the LGI motif of *Drosophila melanogaster* DIAP2 also abolished polyUb binding.

The UBA domains of the IAPs seemed to have a strong preference for highly polymerized forms of Ub (four or more Ub moieties, Fig. 1c–l). Consistently, non-tagged XIAP readily bound to head-to-tail fused tetra-Ub (Fig. 2b), which adopts a similar conformation as that of Lys 63-polyUb chains (D. Komander and D. Barford, personal communication), whereas it failed to bind to monoUb. As XIAP bound exclusively to polymerized forms of Ub, we explored whether polyUb-binding is entirely a consequence of the UBA domain. Although the UBA domain was necessary for Ub-binding, it was not sufficient (Fig. 2c). In isolation, the UBA of XIAP did not bind to polyUb chains, whereas that of Dph1 readily purified polyUb under the same conditions[20] (Fig. 2c). XIAP minimally required the UBA domain and RING finger (Fig. 2d), which mediates homotypic protein interaction[21] and E3 activity (Supplementary Information, Figs S2a, S3). XIAP oligomerization, but not E3 activity, was essential for Ub-binding as $XIAP^{F495A}$, which retains its ability to dimerize but lacks E3 activity (see Supplementary Information, FigS2a and S3), readily bound to polyUb chains (Supplementary Information, Fig. S2b). In contrast, $XIAP^{\Delta C8}$, which lacks the C-terminal eight amino acids and fails to dimerize[21], also failed to interact with polyUb chains (Supplementary Information, Fig. S2a, b). Similarly, the RING finger of cIAP1 was necessary for polyUb-binding (Fig. 2e) as its deletion abolished Ub association. Thus, higher-order oligomeric forms of IAPs are required to allow UBA-dependent binding to polyUb.

Next we examined the importance of the UBA domain in different IAP functions, exemplified by cIAP1, cIAP2–MALT1 and XIAP. Recent studies have shown that cIAP1 is required for proper NF-κB regulation and suppression of caspase-8-mediated apoptosis during TNF-α signalling[7–9,13]. Genetic deletion of cIAP1 results in activation of NF-κB and sensitization to TNF-α-stimulated apoptosis[6]. To determine the role of Ub-binding for cIAP1 function, we reconstituted $cIAP1^{-/-}$ knockout mouse embryonic fibroblasts (MEFs) with inducible $cIAP1^{WT}$ or $cIAP1^{MF/AA}$ rescue (iResc) constructs, and examined their sensitivity to TNF-α killing. Induced expression of $cIAP1^{WT}$ restored resistance to TNF-α (ref. [7] and Fig. 3a) but induction of $cIAP1^{MF/AA}$ failed to provide any protection against TNF-α-mediated cell death, despite comparable expression levels of $cIAP1^{MF/AA}$ and $cIAP1^{WT}$.

cIAP1 is required for endothelial cell survival in developing zebrafish[22]. Null mutants for z-cIAP1 show specific vascular defects caused by caspase-8-dependent apoptosis of endothelial cells, referred to as *tomato* mutant phenotype (Fig. 3b). Re-introduction of $z\text{-}cIAP1^{WT}$ rescued the *tomato* phenotype but $z\text{-}cIAP1^{MF/AA}$ failed to provide any protection from apoptosis of endothelial cells (Fig. 3d–f). Similarly, the Ub ligase-defective $z\text{-}cIAP1^{F645A}$, which is deficient in E3 activity, also failed to rescue the *tomato* mutant phenotype (Fig. 3f). These data indicate that both Ub binding and Ub ligase activity are required for proper cIAP1 function in vertebrates.

Genomic amplification of 11q22, which contains *cIAP1*, occurs at a high frequency in human cancers[23]. Consistent with the notion that cIAP1 functions as a *bona fide* oncogene, deregulated levels of cIAP1 drives tumour formation in cooperation with loss of p53 and expression of c-Myc[23]. To assess the role of the UBA domain in cIAP1-mediated tumorigenesis, we used a transplantation-based mouse model of mosaic liver cancer[24]. Immortalized and p53-deficient liver cells expressing c-Myc were infected with $cIAP1^{WT}$ or $cIAP1^{MF/AA}$. Both constructs expressed cIAP1 protein at comparable levels (Fig. 3g). The infected cells were subsequently

injected into immunocompromised mice to form subcutaneous tumours. Whereas *cIAP1*^{WT} produced tumours with the pathological features of hepatocellular carcinoma[24] (Fig. 3g, h), *cIAP1*$^{MF/AA}$ failed to drive tumour progression under the same conditions.

Importantly, mutation of the UBA domain did not impair the Ub ligase activity of cIAP1. Both wild-type and cIAP1$^{MF/AA}$ retained E3 activity (Supplementary Information, Fig. S4) and were degraded upon treatment with small pharmacological inhibitors of IAPs (M.D., M.M., J.S. and P.M., unpublished observations). These results indicate that UBA-mediated Ub-binding is required for the ability of cIAP1 to provide protection from TNF-α, endothelial cell survival and oncogenic potential.

XIAP is a potent physiological inhibitor of caspase-3, -7 and -9 (ref. 25). In addition, XIAP has also been shown to mediate NF-κB and MAP kinase activation during TGF-β and BMP receptor signalling[26,27], and also with Smac-mimetic treatment and ectopic expression[12,13,28]. To assess the role of the UBA domain in caspase regulation, we used an *in vitro* caspase assay, in which addition of cytochrome c and dATP to cell lysates triggers apoptosome-mediated caspase activation. Both XIAP^{WT} and XIAP$^{\Delta UBA}$ were equally potent in suppressing caspases in this system (Supplementary Information, Fig. S5). Although the UBA domain was dispensable for caspase inhibition, it was involved in XIAP-mediated activation of the NF-κB pathway. Expression of XIAP^{WT} triggered NF-κB activation in a concentration-dependent manner[12,28] (Fig. 4b; Supplementary Information, Fig. S6). However, NF-κB activation by XIAP$^{\Delta UBA}$ and XIAP$^{MF/LL}$ was impaired (Fig. 4c; Supplementary Information, Fig. S6a). The UBA domain mutants XIAP$^{\Delta UBA}$ and XIAP$^{MF/LL}$ were as compromised as the BIR1 mutant XIAP^{V80D}, which fails to bind TAB1 and activate NF-κB[28]. Disruption of Ub ligase activity of XIAP^{F495A} completely abolished NF-κB activation[26] (Fig. 4c). As with cIAP1, the UBA domain of XIAP was not required for E3 activity or dimerization/oligomerization (Supplementary Information, Figs S2a, S3). XIAP$^{MF/AA}$ and XIAP$^{\Delta UBA}$ readily formed dimers, whereas XIAP lacking the extreme C terminus (XIAP$^{\Delta C8}$) failed to oligomerize, which is consistent with previous observations[21]. Further, to examine whether the UBA domain contributes to NF-κB activation through Ub-binding, we substituted the UBA domain of XIAP with that of cbl-b[29] (XIAP$^{cbl\text{-}b\text{-}UBA}$). Intriguingly, the UBA domain of cbl-b was fully functional in the context of XIAP and substituted UBA domain of XIAP for NF-κB activation. XIAP$^{cbl\text{-}b\text{-}UBA}$ was even more potent in activating NF-κB (Supplementary Information, Fig. S6b). Together, these data indicate that the Ub-binding ability of XIAP and E3 activity are both required for efficient activation of NF-κB.

Reciprocal chromosomal translocation of *cIAP2* and the paracaspase *MALT1* gene is the most prevalent chromosomal aberration associated with MALT lymphoma11. The resulting cIAP2–MALT1 fusion protein drives B-cell transformation and lymphoma progression through constitutive activation of NF-κB11,15. Under normal conditions, T- and B-cell antigen receptor stimulation triggers MALT1 oligomerization through Bcl10. This leads to TRAF6-mediated Lys 63-polyubiquitylation of NEMO (IKKγ) and NF-κB activation. The requirement for Bcl10 and upstream signals is bypassed in the cIAP2–MALT1 chimaera, as the BIR1 of cIAP2 maintains cIAP2–MALT1 in a constitutively dimerized/oligomerized state[30] (V. Dixit, personal communication) and thereby triggers Lys 63-linked polyubiquitylation of NEMO, presumably by recruiting the Ub ligase TRAF6 and Ub-conjugating enzyme (E2) Ubc13/Uev1a30,31.

By mechanisms not fully understood, ubiquitylation of NEMO triggers activation of IKKα/β, causing phosphorylation and degradation of I B, release of NF-κB and, ultimately, transcription of target genes[30,32,33]. The BIR1 domain of cIAP2 reportedly is necessary and sufficient for oligomerization of cIAP2–MALT1 and NF-κB activation[30]. However, in 98% of all reported cases the breakpoint in the *cIAP2* gene occurs downstream of exon 7 (ref. 34), which encodes

the UBA domain (Fig. 4d, exon numbering as previously described35). The breakpoint frequency downstream of exon 7 in *cIAP2* and the consistency of 'in-frame' cIAP2–MALT1 fusions strongly suggest that the UBA domain is required for the full oncogenic potential of cIAP2–MALT1. Notably, analysis of the sequences near the breakpoint junctions did not provide any evidence for the participation of site-specific recombination, pointing to a selective advantage for the inclusion of exon 7 (ref. 34).

To examine the functionality of the UBA domain in cIAP2–MALT1, we tested various mutants of the case4 variant of the cIAP2–MALT1 chimaera for their ability to induce NF-κB activation (Fig. 4e, f). cIAP2–MALT1^{WT} readily stimulated NF-κB activation, whereas the UBA mutant cIAP2–MALT1$^{MF/AA}$ failed to induce NF-κB activation under the same conditions. Similarly, cIAP2–MALT1$^{\Delta BIR1}$, which lacks the BIR1 domain also failed to activate NF-κB (Fig. 4e, f). The N-terminal cIAP2 region and the C-terminal MALT1 portion on their own were unable to induce NF-κB activation[36]. These results show that both the UBA and BIR1 domain are required for NF-κB activation by the case4 variant of the cIAP2–MALT1 fusion protein.

To gain insight into the molecular mechanism through which the UBA domain contributes to IAP-mediated signalling, we used cIAP2–MALT1 as a model system. First, we tested the ability of cIAP2–MALT1 to bind to Ub conjugates *in vivo* (Fig. 5a). cIAP2–MALT1^{WT} readily co-purified Ub-conjugated proteins from cellular extracts, whereas cIAP2–MALT1$^{MF/AA}$ failed to interact efficiently with Ub conjugates. This indicates that the UBA domain endows cIAP2–MALT1 with the ability to interact with Ub.

Lys 63-linked polyubiquitylation of NEMO is important for cIAP2–MALT1-mediated activation of NF-κB[30]. Because NF-κB activation by the UBA domain mutant of cIAP2–MALT1 was severely impaired, we first examined whether this domain contributes to NEMO polyubiquitylation. We found that cIAP2–MALT1$^{MF/AA}$ induced polyubiquitylation of NEMO as efficiently as cIAP2–MALT1^{WT} (Fig. 5b). The ability of cIAP2–MALT1 to oligomerize was also not affected by mutations in the UBA domain (Fig. 5c). This indicates that the UBA domain is not required for NEMO ubiquitylation or cIAP2–MALT1 oligomerization. This is in contrast to cIAP2–MALT1$^{\Delta BIR1}$, which disrupts both self-oligomerization and cIAP2–MALT1-mediated ubiquitylation of NEMO[30,36] (Fig. 5b, c). Our data indicate, therefore, that Lys 63-polyubiquitylation of NEMO, although essential, is not sufficient for cIAP2–MALT1 to induce NF-κB activation. Thus, cIAP2–MALT1-mediated activation of NF-κB results from a Ub-binding-dependent activity.

To investigate whether the UBA domain contributes to NF-κB activation by trapping Lys 63-polyUb–NEMO conjugates, we tested the ability of cIAP2–MALT1^{WT} and cIAP2–MALT1$^{MF/AA}$ to bind to either unmodified or ubiquitylated forms of NEMO. Purified cIAP2–MALT1 proteins were incubated with cell lysates containing either non-ubiquitylated or polyubiquitylated forms of NEMO-V5. Unmodified NEMO associated with both cIAP2–MALT1^{WT} and cIAP2–MALT1$^{MF/AA}$ indiscriminately, whereas polyUb–NEMO interacted strongly with cIAP2–MALT1^{WT} but not cIAP2–MALT1$^{MF/AA}$ (Fig. 5d). Notably, cIAP2–MALT1^{WT} bound preferentially to polyUb–NEMO, as the amount of co-purified polyUb–NEMO was strongly enriched, compared with the unmodified form in the pulldown assays (Fig. 5d, compare the ratio of polyUb–NEMO to unmodified NEMO in lane 2 and lane 7). Furthermore, cIAP2–MALT1^{WT}, but not cIAP2–MALT1$^{MF/AA}$, purified polyubiquitylated endogenous NEMO from cellular extracts (Fig. 5e). As NEMO harbours a ubiquitin-binding domain (UBD), it is possible that this domain contributes to cIAP2–MALT1 binding by interacting with polyUb chains on cIAP2–MALT1. To examine this possibility we repeated the above experiment with *NEMO^{D311N}*, which carries a point mutation in the UBD that abrogates Ub binding[37] (Supplementary Information, Fig. S7). However, cIAP2–MALT1 enriched polyubiquitylated forms of NEMO^{D311N} as efficiently as NEMO^{WT} (Fig. 5f),

indicating that the UBD of NEMO is not required for binding to cIAP2–MALT1^{WT}. Moreover, the polyubiquitylation status of wild-type and UBA domain mutant cIAP2–MALT1 were indistinguishable (Supplementary Information, Fig. S8), ruling out the possibility that differences in cIAP2–MALT1 polyubiquitylation account for differential polyUb–NEMO binding. Therefore, these data are consistent with the notion that the UBA domain of cIAP2–MALT1 mediates binding to polyubiquitylated NEMO and is not required for initial recruitment or ubiquitylation of unmodified NEMO.

In conclusion, we have identified a previously undescribed UBA domain in IAP family members that enables them to interact with Lys 63-linked polyUb chains. The notion that the UBA domain is evolutionarily conserved in several IAPs, such as mammalian cIAP1, cIAP2, XIAP and *Drosophila* DIAP2, indicates that it has an important physiological function. Consistently, we find that the UBA domain is essential for cIAP1, XIAP and cIAP2–MALT1 to take part in signalling processes leading to NF-κB activation, cell survival and tumorigenesis. It is tempting to speculate that the UBA domain of cIAP1, cIAP2 and XIAP enables these IAPs to modulate NF-κB signalling by binding to ubiquitylated RIP1 or NEMO.

METHODS

Affinity reagents

The following antibodies were used according to manufacturers' instructions: anti-HA (1:2000; Roche Diagnostics, Burgess Hill, UK), α-FLAG–HRP (1:5000; Sigma-Aldrich), anti-c-Myc (1:1000; Santa Cruz Biotechnology), anti-V5 (1:2000; AbD Serotec), anti-GST (1:2000; Novus Biologicals), anti-Ub (1:100; Sigma-Aldrich), mouse monoclonal anti-XIAP (1:1000; BD Biosciences), rabbit polyclonal anti-XIAP (to detect XIAPDUBA; 1:1000; Cell Signaling Technology), rabbit polyclonal anti-cIAP1 (1:200; Abcam), anti-cIAP1 (1:2000; ref. 38), anti-NEMO (1:1000; Santa Cruz Biotechnology), anti-caspase-3 (1:1000; Cell Signaling Technology), anti-caspase-9 (1:2000; R&D Systems), anti-actin (1:1000; Santa Cruz Biotechnology), anti-tubulin (1:1000; Santa Cruz Biotechnology) antibodies, Strep-Tactin-Sepharose resin (IBA), anti-HA-agarose resin (Sigma-Aldrich), anti-FLAG-agarose resin (Sigma Aldrich), anti-V5-agarose resin (Sigma-Aldrich), glutathione-sepharose resin (GE healthcare).

Plasmids and cloning

pRK5B–FLAG–cIAP2–MALT1 and the NF-κB luciferase reporter plasmid, pBIIX–Luc, have been described previously[39,40]. pEX105–IBA–Strep–Ub was a gift from Marja Jäättelä (Danish Cancer Society, Copenhagen, Denmark). Human 3×HA–Ub cDNA was cloned into pcDNA3. In general, pcDNA3-based constructs were generated by PCR and specific point-mutants created by site-directed mutagenesis (Stratagene), according to the manufacturer's instructions. For *in vivo* tumour formation experiments, 6×Myc–cIAP1 or –cIAP1$^{MF/AA}$ cDNAs were cloned into MSCV–IRES–GFP. All GST-fusion constructs were generated by PCR and cloned into pGEX-6P-1. cIAP1 WT and MF/AA were cloned into a pF 5x UAS SV40 Puro vector. All constructs were verified by DNA sequencing.

Purification of recombinant proteins

GST-tagged XIAP, cIAP1, cIAP2 and DIAP2 proteins were expressed in bacteria in the presence of 0.2 mM isopropyl β-D-1-thiogalactopyranoside (IPTG) and 200 μM $ZnSO_4$ for 16 h at 16 °C. $ZnSO_4$ was added to ensure better folding of the Zn-coordinating BIR and RING domains. Because of problems producing soluble full-length proteins, we used the C-terminal portion of cIAP1 (residues 383–612), cIAP2 (residues 373–604) and DIAP2 (residues 313–498) for the Ub-binding assays. XIAP was full length. After induction, bacteria were resuspended in phosphate-buffered saline (PBS) containing 300 mM NaCl, 1 mM dithiothreitol

(DTT) and protease inhibitor mix (Roche Diagnostics), and lysed by sonication. Proteins were captured on reduced glutathione-sepharose resin and washed four times in PBS containing 300 mM NaCl. Finally, GST-fusion proteins were eluted with 50 mM TrisHCl (pH 8.0) containing 12.5 mM reduced glutathione for 30 min at room temperature. Recombinant XIAP proteins used in the *in vitro* apoptosome assay and GST-tagged Ub binding assay were purified by cleaving off the GST-tag using PreScission protease (GE Healthcare). Eluates were dialysed against PBS, 1 mM DTT was added and recombinant proteins were stored at −80° C.

In vitro Ub binding assay

Ub-binding assays were conducted as described previously[17,19]. For more details see the Supplementary Information.

NF-κB reporter assays

HEK293T cells were co-transfected with the NF-κB reporter plasmid and the indicated cIAP2–MALT1 or XIAP constructs. After 24 h, cells were lysed in 200 μl passive lysis buffer (Promega) and luciferase activity measured using the Luciferase Assay System (Promega) according to manufacturer's instructions.

Purification of Ub conjugates

One confluent 35-mm dish of HEK293T cells for each condition, transfected as indicated, was lysed in 400 μl ice cold Ub lysis buffer on ice (25 mM HEPES (4-(2-hydroxyethyl)-1-piperazineethanesulfonic acid; pH 7.4), 150 mM KCl, 2 mM $MgCl_2$, 1 mM EGTA (ethylene glycol tetraacetic acid), 0.5% Triton X-100) containing 50 mM iodoacetamide. Lysates were cleared by centrifugation and incubated with 25 μl Strep-Tactin-Sepharose resin. Samples were incubated for 2 h at 4 ° C, washed four times in 500 μl lysis buffer and bound material was eluted with 75 μl D-desthiobiotin buffer (IBA). Sample buffer was added and samples subjected to SDS–PAGE and immunoblotting.

HA–Ub-conjugate binding and polyUb–NEMO binding assays

For each condition, HEK293T cells (one 6-cm dish) were transiently transfected with HA-tagged Ub, alone (Fig. 5a) or with NEMO-V5 (Fig. 5d, lanes 1 and 3–5) or with NEMO-V5 plus XIAP (XIAP induces strong ubiquitylation of NEMO (M.G.-H. and P.M., unpublished observation); Fig. 5d) and lysed in 400 μl ice cold Ub lysis buffer containing 50 mM iodoacetamide on ice. Lysate was cleared by centrifugation. In parallel, one 6-cm dish HEK293T cells for each condition were transfected with the indicated FLAG-tagged cIAP2–MALT1 plasmids. After 24 h, cells were lysed in 400 μl ice cold Ub lysis buffer and incubated with anti-FLAG-agarose resin (Sigma). Samples were washed three times in 500 μl Ub lysis buffer and the cleared lysates were added. After incubation for 1 h at 4 °C, samples were washed four times in 500 μl Ub lysis buffer. Bound material was eluted in 75 μl of glycine (0.2 M, pH 2.5), sample buffer was added and samples were subjected to SDS–PAGE and immunoblotting. To detect an interaction between cIAP2–MALT1 and endogenous NEMO, two 10-cm dish of HEK293T cells per condition were transfected with FLAG–cIAP2–MALT1 and HA-tagged Ub. After 24 h, cells were lysed in 1.2 ml ice-cold lysis buffer containing 50 mM iodoacetamide on ice. FLAG–cIAP2–MALT1 was immunoprecipitated and samples were processed as described above.

cIAP1$^{-/-}$ reconstitution assays in mouse and zebrafish, and generation/characterization of liver carcinomas

Knockout MEFs were generated from E15 cIAP1$^{-/-}$ mouse embryos, using standard procedures, and infected with SV40 large T antigen-expressing lentivirus[7]. To generate lentiviral particles, 293T cells were transfected with the packaging constructs pCMV δR8.2,

VSVg and the relevant lentiviral plasmid in a ratio of 1:0.4:0.6. After 24–48 h, the virus-containing supernatants were collected and filtered (0.45 μm). Polybrene (4 μg ml^{-1}) was added and target cells infected with virus supernatant for 24–48 h. The medium was subsequently changed and successful infection selected for with puromycin (2–5 μg ml^{-1}: pF 5 × UAS selection) or hygromycin B (100–300 μg ml^{-1}: GEV16 selection). pF 5 × UAS-inducible constructs were induced with 4-hydroxy tamoxifen (4HT, 100 nM) for 24 h before collecting lysates for western blotting and 72 h before death assays. The zebrafish rescue experiments were performed as described previously[20]. Briefly, embryos from *tom*^{s805} heterozygote intercrosses were injected at the one- or two-cell stage with the indicated amount of mRNA encoding for the different cIAP1 mutants, and scored for *tomato* phenotype at 60–72 h post-fertilization (hpf). At least one hundred eggs were injected for each experimental point. Data shown are the means of three independent experiments for each construct. Isolation of embryonic hepatoblasts, culturing and retroviral transduction were performed as described previously[23]. $p53^{-/-}$ hepatoblasts (embryonic day 18) were infected with c-Myc at low MOI to generate immortalized liver cell lines (L.Z. and S.L., manuscript in preparation). For subcutaneous tumour growth, 2×10^6 cells were infected with cIAP1^{WT} or cIAP1$^{MF/AA}$, injected into flanks of nude mice and monitored as described previously[23]. Haematoxylin and eosin (H&E) staining was performed on paraffin-embedded tumour sections.

In vivo cell death assay

Cells were seeded on 12-well tissue culture plates at approximately 10% confluency and were allowed to adhere for 8 h before addition of 4HT. Cells were treated with 4HT for 72 h, followed by the addition of human Fc-TNF-α (100 ng ml^{-1}) for 24 h. Cell death was measured by propidium iodide (PI) staining and flow cytometry. In each sample 10,000 events were measured, and cell death (% PI-positive cells) quantified.

Supplementary Material

Refer to Web version on PubMed Central for supplementary material.

Acknowledgments

We would like to thank Xiaolu Yang, David Komander, David Barford, Thomas Farkas, Ivan Dikic and Marja Jaattela for reagents, discussions and invaluable technical support. We thank Irene Scarfò for help with the cIAP1 zebrafish experiments, and Hyejin Cho and Beicong Ma for excellent technical assistance and help with the mouse tumour model. We thank Alan Ashworth and members of the Meier laboratory for critical reading of the manuscript and helpful discussions. We thank Vishva Dixit for sharing unpublished results. M.G.-H. is supported by a fellowship from the Danish Cancer Society. M.M.S. is supported by a HFSP Career Developmental Award, Fondazione San Paolo and Regione Piemonte.

References

1. Di Fiore PP, Polo S, Hofmann K. When ubiquitin meets ubiquitin receptors: a signalling connection. Nature Rev Mol Cell Biol 2003;4:491–497. [PubMed: 12778128]
2. Hoeller D, Hecker CM, Dikic I. Ubiquitin and ubiquitin-like proteins in cancer pathogenesis. Nature Rev Cancer 2006;6:776–788. [PubMed: 16990855]
3. Hunter AM, LaCasse EC, Korneluk RG. The inhibitors of apoptosis (IAPs) as cancer targets. Apoptosis 2007;12:1543–1568. [PubMed: 17573556]
4. Cook WJ, Jeffrey LC, Sullivan ML, Vierstra RD. Three-dimensional structure of a ubiquitin-conjugating enzyme (E2). J Biol Chem 1992;267:15116–15121. [PubMed: 1321826]
5. Varadan R, et al. Solution conformation of Lys 63-linked di-ubiquitin chain provides clues to functional diversity of polyubiquitin signaling. J Biol Chem 2004;279:7055–7063. [PubMed: 14645257]
6. Salvesen GS, Duckett CS. Apoptosis: IAP proteins: blocking the road to death's door. Nature Rev Mol Cell Biol 2002;3:401–410. [PubMed: 12042762]

7. Vince JE, et al. IAP antagonists target cIAP1 to induce TNF-α-dependent apoptosis. Cell 2007;131:682–693. [PubMed: 18022363]
8. Varfolomeev E, et al. IAP antagonists induce auto-ubiquitination of c-IAPs, NF-κB activation, and TNF-α-dependent apoptosis. Cell 2007;131:669–681. [PubMed: 18022362]
9. Petersen SL, et al. Autocrine TNF-α signaling renders human cancer cells susceptible to Smac-mimetic-induced apoptosis. Cancer Cell 2007;12:445–456. [PubMed: 17996648]
10. Li X, Yang Y, Ashwell JD. TNF-RII and c-IAP1 mediate ubiquitination and degradation of TRAF2. Nature 2002;416:345. [PubMed: 11907583]
11. Isaacson PG, Du MQ. Gastrointestinal lymphoma: where morphology meets molecular biology. J Pathol 2005;205:255–274. [PubMed: 15643667]
12. Hofer-Warbinek R, et al. Activation of NF-κ B by XIAP, the X chromosome-linked inhibitor of apoptosis, in endothelial cells involves TAK1. J Biol Chem 2000;275:22064–22068. [PubMed: 10807933]
13. Gaither A, et al. A Smac mimetic rescue screen reveals roles for inhibitor of apoptosis proteins in tumor necrosis factor-alpha signaling. Cancer Res 2007;67:11493–11498. [PubMed: 18089776]
14. Bertrand MJ, et al. cIAP1 and cIAP2 facilitate cancer cell survival by functioning as E3 ligases that promote RIP1 ubiquitination. Mol Cell 2008;30:689–700. [PubMed: 18570872]
15. Lucas PC, et al. Bcl10 and MALT1, independent targets of chromosomal translocation in malt lymphoma, cooperate in a novel NF-κB signaling pathway. J Biol Chem 2001;276:19012–19019. [PubMed: 11262391]
16. Kirkin V, Dikic I. Role of ubiquitin- and Ubl-binding proteins in cell signaling. Curr Opin Cell Biol 2007;19:199–205. [PubMed: 17303403]
17. Swanson KA, Hicke L, Radhakrishnan I. Structural basis for mono-ubiquitin recognition by the Ede1 UBA domain. J Mol Biol 2006;358:713–724. [PubMed: 16563434]
18. Ohno A, et al. Structure of the UBA domain of Dsk2p in complex with ubiquitin molecular determinants for ubiquitin recognition. Structure 2005;13:521–532. [PubMed: 15837191]
19. Raasi S, Orlov I, Fleming KG, Pickart CM. Binding of polyubiquitin chains to ubiquitin-associated (UBA) domains of HHR23A. J Mol Biol 2004;341:1367–1379. [PubMed: 15321727]
20. Raasi S, Varadan R, Fushman D, Pickart CM. Diverse polyubiquitin interaction properties of ubiquitin-associated domains. Nature Struct Mol Biol 2005;12:708–714. [PubMed: 16007098]
21. Silke J, et al. The anti-apoptotic activity of XIAP is retained upon mutation of both the caspase-3- and caspase-9-interacting sites. J Cell Biol 2002;157:115–124. [PubMed: 11927604]
22. Santoro MM, Samuel T, Mitchell T, Reed JC, Stainier DY. Birc2 (cIap1) regulates endothelial cell integrity and blood vessel homeostasis. Nature Genet 2007;39:1397–1402. [PubMed: 17934460]
23. Zender L, et al. Identification and validation of oncogenes in liver cancer using an integrative oncogenomic approach. Cell 2006;125:1253–1267. [PubMed: 16814713]
24. Zender L, et al. Generation and analysis of genetically defined liver carcinomas derived from bipotential liver progenitors. Cold Spring Harb Symp Quant Biol 2005;70:251–261. [PubMed: 16869761]
25. Eckelman BP, Salvesen GS, Scott FL. Human inhibitor of apoptosis proteins: why XIAP is the black sheep of the family. EMBO Rep 2006;7:988–994. [PubMed: 17016456]
26. Birkey Reffey S, Wurthner JU, Parks WT, Roberts AB, Duckett CS. X-linked inhibitor of apoptosis protein functions as a cofactor in transforming growth factor-β signaling. J Biol Chem 2001;276:26542–26549. [PubMed: 11356828]
27. Yamaguchi K, et al. XIAP, a cellular member of the inhibitor of apoptosis protein family, links the receptors to TAB1-TAK1 in the BMP signaling pathway. EMBO J 1999;18:179–187. [PubMed: 9878061]
28. Lu M, et al. XIAP induces NF-κB activation via the BIR1/TAB1 interaction and BIR1 dimerization. Mol Cell 2007;26:689–702. [PubMed: 17560374]
29. Peschard P, et al. Structural basis for ubiquitin-mediated dimerization and activation of the ubiquitin protein ligase Cbl-b. Mol Cell 2007;27:474–485. [PubMed: 17679095]

30. Zhou H, Du MQ, Dixit VM. Constitutive NF-κB activation by the t(11;18) (q21;q21) product in MALT lymphoma is linked to deregulated ubiquitin ligase activity. Cancer Cell 2005;7:425–431. [PubMed: 15894263]

31. Noels H, et al. A Novel TRAF6 binding site in MALT1 defines distinct mechanisms of NF-κB activation by API2middle dotMALT1 fusions. J Biol Chem 2007;282:10180–10189. [PubMed: 17287209]

32. Zhou H, et al. Bcl10 activates the NF-κB pathway through ubiquitination of NEMO. Nature 2004;427:167–171. [PubMed: 14695475]

33. Sun L, Deng L, Ea CK, Xia ZP, Chen ZJ. The TRAF6 ubiquitin ligase and TAK1 kinase mediate IKK activation by BCL10 and MALT1 in T lymphocytes. Mol Cell 2004;14:289–301. [PubMed: 15125833]

34. Baens M, Steyls A, Dierlamm J, De Wolf-Peeters C, Marynen P. Structure of the MLT gene and molecular characterization of the genomic breakpoint junctions in the t(11;18)(q21;q21) of marginal zone B-cell lymphomas of MALT type. Genes Chromosomes Cancer 2000;29:281–291. [PubMed: 11066071]

35. Young SS, et al. Genomic organization and physical map of the human inhibitors of apoptosis: HIAP1 and HIAP2. Mamm Genome 1999;10:44–48. [PubMed: 9892732]

36. Lucas PC, et al. A dual role for the API2 moiety in API2-MALT1-dependent NF-κB activation: heterotypic oligomerization and TRAF2 recruitment. Oncogene 2007;26:5643–5654. [PubMed: 17334391]

37. Wu CJ, Conze DB, Li T, Srinivasula SM, Ashwell JD. Sensing of Lys 63-linked polyubiquitination by NEMO is a key event in NF-κB activation [corrected]. Nature Cell Biol 2006;8:398–406. [PubMed: 16547522]

38. Silke J, et al. Determination of cell survival by RING-mediated regulation of inhibitor of apoptosis (IAP) protein abundance. Proc Natl Acad Sci USA 2005;102:16182–16187. [PubMed: 16263936]

39. Hu S, et al. cIAP2 is a ubiquitin protein ligase for BCL10 and is dysregulated in mucosa-associated lymphoid tissue lymphomas. J Clin Invest 2006;116:174–181. [PubMed: 16395405]

40. Li M, et al. An essential role of the NF-κ B/Toll-like receptor pathway in induction of inflammatory and tissue-repair gene expression by necrotic cells. J Immunol 2001;166:7128–7135. [PubMed: 11390458]

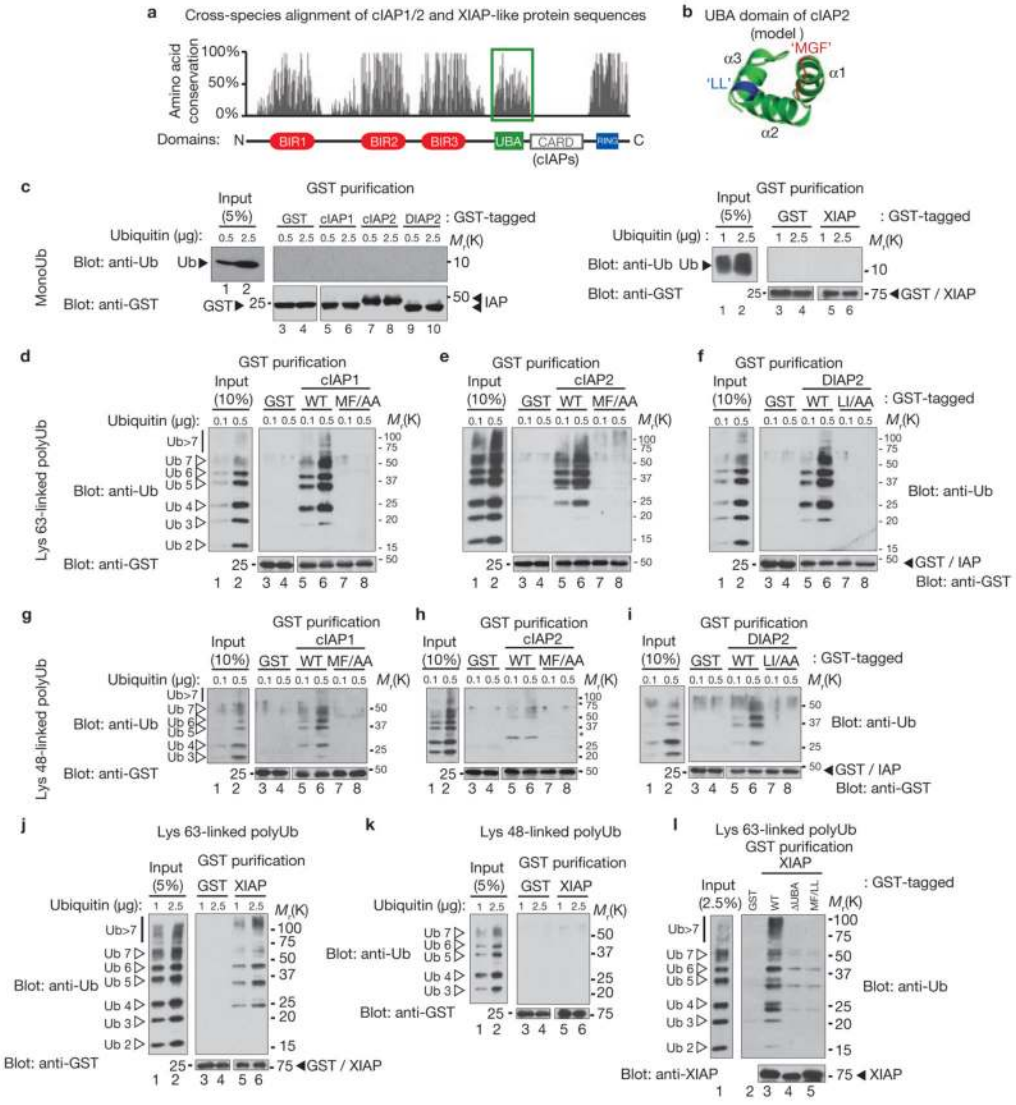

Figure 1.

IAPs carry an evolutionarily conserved UBA domain that mediates Ub binding. (**a**) Graph shows conservation of amino acid residues of IAPs of the cIAP- and XIAP subtype ranging from *Drosophila* to humans (see Supplementary Information, Fig. S1 for details). The UBA domain is highlighted in green. Shown below is a schematic representation of cIAPs indicating the location of the UBA domain. (**b**) Predicted 3D structure of the cIAP2 UBA domain. The 3D structure was modelled with the help of the solution structure of RSGI RUH-011, a UBA domain from *Arabidopsis* cDNA (PDB code 1vek), as it is the best modelling template for the 3D structure of cIAP2 UBA domain (statistically significant Pcons score 1.250), followed by three other structures (2cpw, 1whc, and 2dkl, see Supplementary Information for details) (**c**–**l**) Purified recombinant GST-tagged XIAP, cIAP1, cIAP2 and DIAP2 were immobilized on glutathione-sepharose resin. The indicated monoUb (**c**) Lys 48-linked (**d**–**f**, **k**) or Lys 63-linked (**g**–**j**, **l**) polyUb chains were added and Ub-binding was assayed by immunoblotting the bound fractions with an anti-Ub antibody. The presence of the GST–IAP was verified by immunoblotting with an anti-GST (**c**–**k**) or anti-XIAP (**l**) antibody.

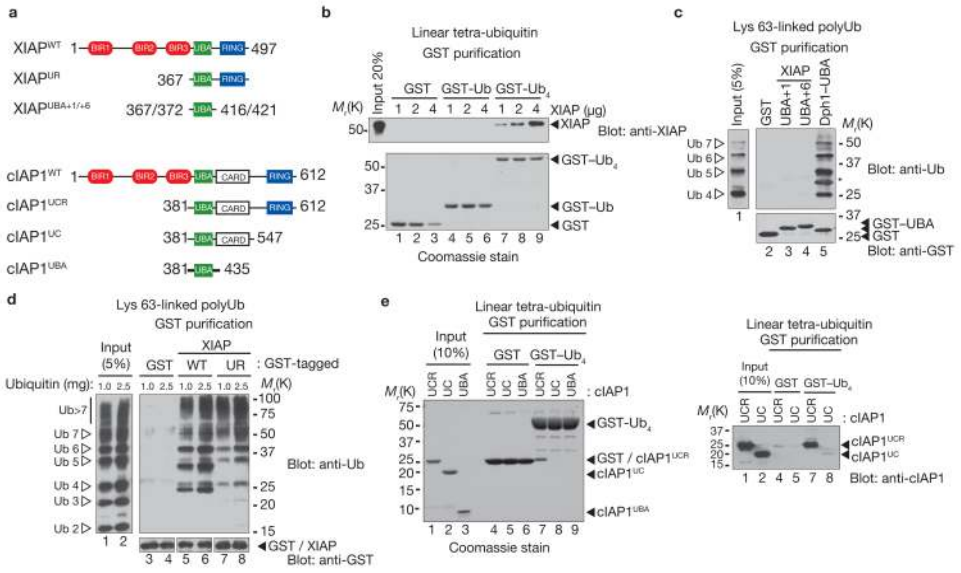

Figure 2.

RING-mediated dimerization of XIAP and cIAP1 is required for Ub binding. (**a**) Schematic representation of the constructs used. (**b**) Purified recombinant GST, GST-tagged monoUb and linear tetra-Ub (Ub_4) were immobilized on glutathione-sepharose resin. The indicated amounts of recombinant XIAP were added and the retention of XIAP was assayed by immunoblotting the bound fractions with an anti-XIAP antibody. The presence of GST, GST–Ub and GST–Ub_4 was verified by Coomassie staining. (**c**, **d**) Ub-binding assays were performed as described in Fig. 1. (**e**) Purified recombinant GST or linear Ub_4 were immobilized on glutathione-sepharose resin. Recombinant untagged cIAP1 fragments were added and the retention of cIAP1 was assayed by Coomassie staining and immunoblotting the bound fractions with an anti-cIAP1 antibody.

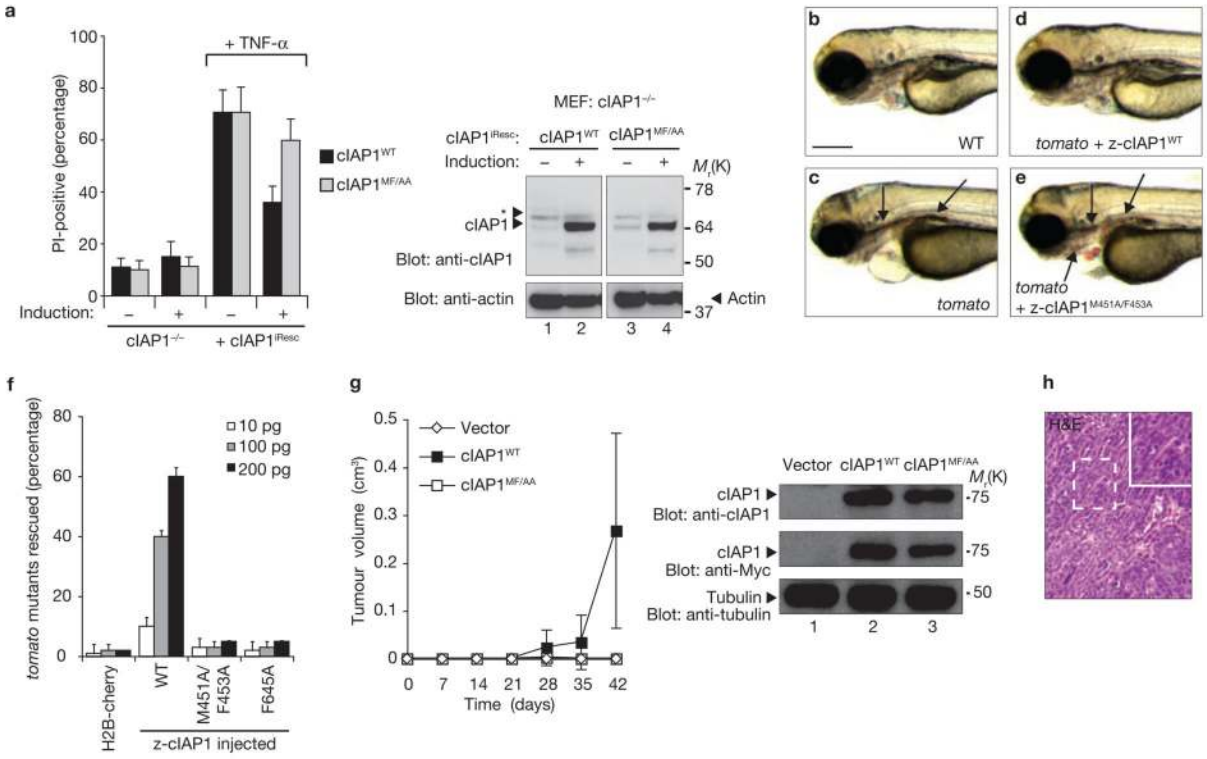

Figure 3.

The UBA is required for IAP function. (**a**) Inducible cIAP1^{WT}, but not cIAP1$^{MF/AA}$, blocks sensitivity of *cIAP1* knockout cells to TNF-α. A *cIAP1* knockout MEF line was infected with inducible cIAP1 rescue constructs (iResc). Independent clones of *cIAP1*$^{-/-}$ MEFs, reconstituted with either cIAP1^{WT} (n = 11) or cIAP1$^{MF/AA}$ (n = 11) were tested for inducible expression of cIAP1 and sensitivity to TNF-α. Representative immunoblots of lysates from MEFs carrying the inducible-rescue constructs are shown to indicate normal levels of cIAP1. The inducible cIAP1 clones were left uninduced or induced for cIAP1 and then treated with TNF-α for 24 h. Cells were stained with PI and analysed by flow cytometry. Error bars are 2 × s.e.m. throughout. P = 0.0002 (two-tailed t-test) for *cIAP1*$^{MF/AA}$ tested against *cIAP1*^{WT} in induced samples treated with TNF-α. (**b**–**e**) WT but not UBA domain mutant cIAP1 rescues the *tomato (tom)* phenotype caused by loss of z-cIAP1. Embryos from *tom*^{s805} heterozygote intercrosses were injected at the one-cell stage with the indicated amounts of mRNA encoding z-cIAP1, z-cIAP1$^{MF/AA}$ and z-cIAP1^{F645A}. Representative images of wild-type (**b**), *tom* mutants (**c**) and *tom*^{s805} -mutants injected with z-cIAP1^{WT} (**d**) and z-cIAP1$^{MF/AA}$ (**e**) are shown. A control mRNA for H2B–cherry (50 pg) was also used in each injection alone or in addition to the cIAP1 contructs. (**f**) Histograms show the percentage of rescued *tom* mutants identified 72 hpf after injection. P = 0.0010 (10 pg), P = 0.0006 (100 pg), P = 0.0051 (200 pg) for z-cIAP1$^{MF/AA}$ tested against z-cIAP1^{WT}, and P = 0.0010 (10 pg), P = 0.00004 (100 pg), P = 0.0074 (200 pg) for z-cIAP1^{F645A} tested against z-cIAP1^{WT}. Scale bar, 0.25 mm. (**g**, **h**) cIAP1 UBA mutants fail to promote liver tumour formation. p53$^{-/-}$;Myc liver cells were injected subcutaneously into nude mice (**g**). Data are mean ± s.d. (n = 4). P = 0.022 (two-tailed t-test) for cIAP1$^{MF/AA}$ tested against cIAP1^{WT} at 42 day time point after injection. Immunoblots of p53$^{-/-}$;Myc liver cells infected with retrovirus expressing cIAP1^{WT} or cIAP1$^{MF/AA}$ mutant. (**h**) Histopathology of representative tumours from cIAP1^{WT}.

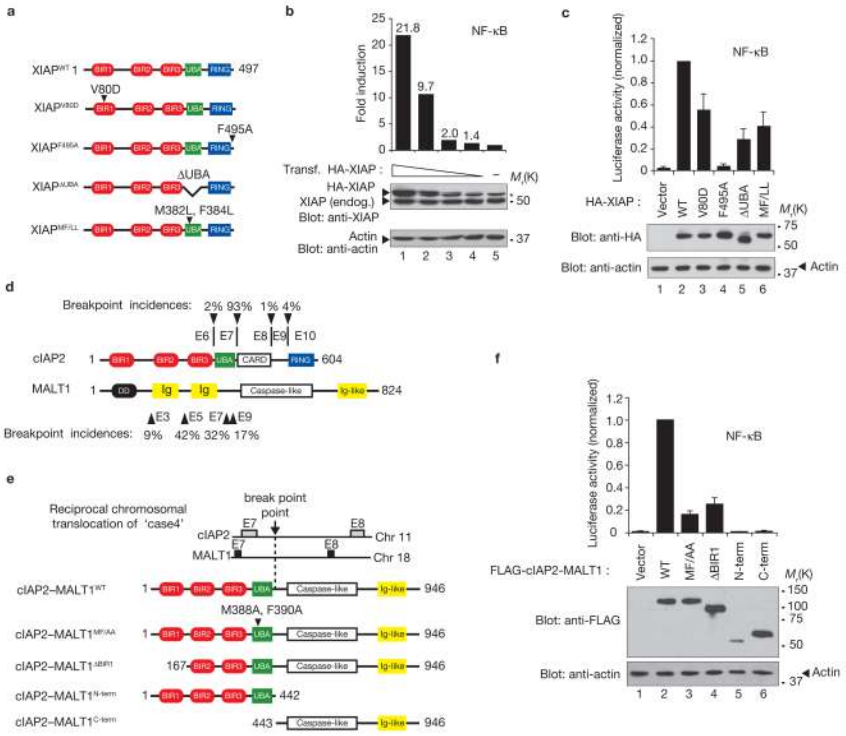

Figure 4.

The ability of XIAP to induce NF-κB is dependent on its UBA domain. (**a**) Schematic representation of the XIAP constructs used. (**b**) Decreasing amounts of *xiap* plasmids (100 ng, 40 ng, 13 ng and 4 ng) and 50 ng of an NF-κB luciferase reporter were co-transfected into HEK293T cells. Data represent mean from one of three independent experiments. Expression levels of XIAP was determined by immunoblotting using anti-XIAP and anti-actin antibodies. The asterisk refers to a cross-reactive band. (**c**) 150 ng of *xiap* plasmids and 50 ng of a NF-κB luciferase reporter were co-transfected into HEK293T cells. Deletion of the UBA domain-like mutation of the MGF motif (MF/LL) abrogates XIAP-mediated NF-κB activation (P = 0.00005 and P = 0.0004, respectively). Similarly, mutation of the BIR1 domain (V80D) or RING finger region (F495A) also abrogated NF-κB signalling (P = 0.008 and $P = 4.9 \times 10^{-7}$, respectively). Of note, the F495A mutation abolishes E3 ligase activity of XIAP (see Supplementary Information, Fig. S3). Data represent mean ± s.d. of four (V80D and F495A) or five independent experiments. Two-tailed t-test was used to determine statistical significance (tested against XIAP^{WT}). (**d**–**f**) The UBA domain is essential for cIAP2–MALT1-mediated NF-κB activation. (**d**) Schematic representation of the position and frequency of the chromosomal breakpoints in *cIAP2* and *MALT1* observed in t(11:18)(q21:q21)-positive MALT-lymphomas. Arrowheads show the exon (E) boundaries and position of breakpoints. (**e**) Schematic representation of cIAP2–MALT1 (case4 variant) used in **f**. (**f**) The indicated cIAP2–MALT1 plasmids and a NF-κB luciferase reporter were co-transfected into HEK293T cells. Luciferase activities are expressed relative to wild-type cIAP2–MALT1. Data represent mean ± s.d. of four independent experiments. Two-tailed t-test was used to determine statistical significance (tested against cIAP2–MALT1^{WT}): MF/AA ($P = 1.4 \times 10^{-5}$), ΔBIR1 ($P = 1.1 \times 10^{-4}$), N-term ($P = 9.7 \times 10^{-11}$), C-term ($P = 1.6 \times 10^{-7}$). Expression levels of cIAP2–MALT1 was determined by immunoblotting using anti-FLAG and anti-actin antibodies.

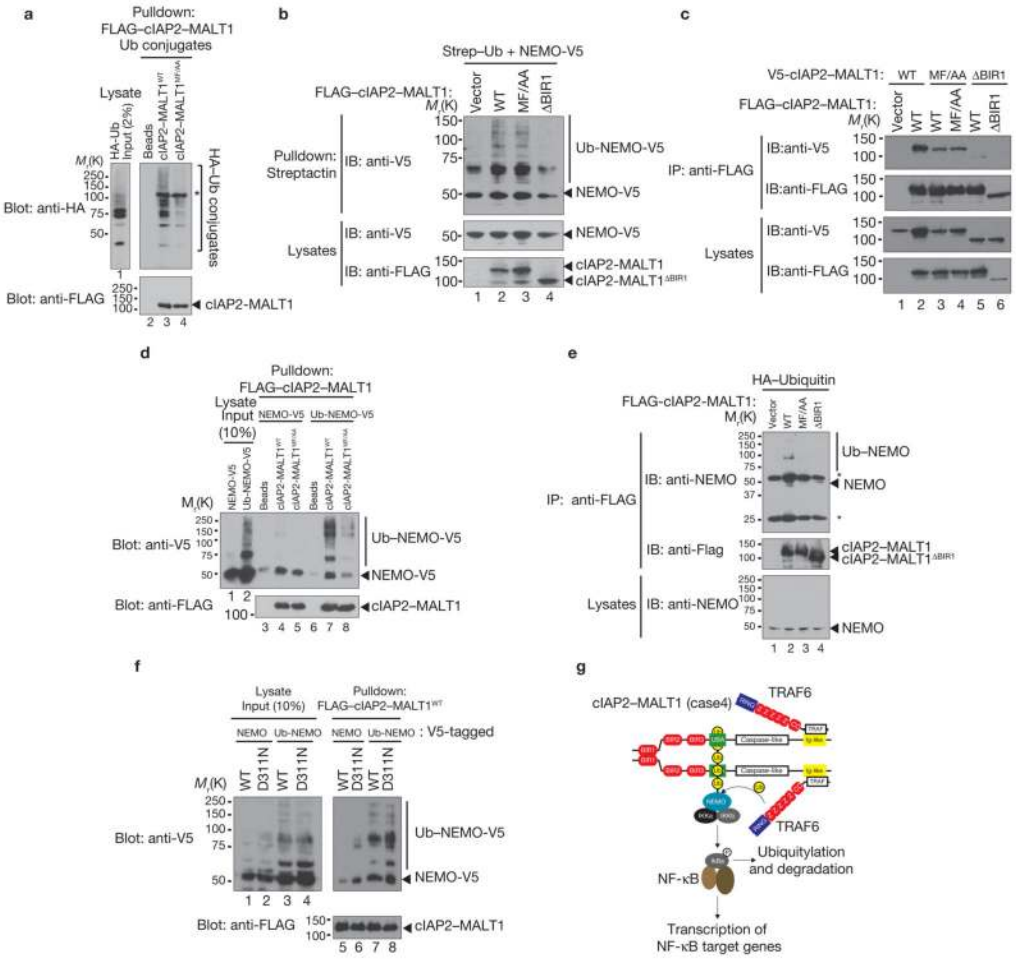

Figure 5.

The UBA domain of cIAP2–MALT1 interacts with polyubiquitylated NEMO. (**a**) cIAP2–MALT1 interacts with Ub conjugates in a UBA-dependent manner. FLAG–cIAP2–MALT1 and FLAG–cIAP2–MALT1$^{MF/AA}$ immobilized on anti-FLAG–agarose resin were used to pull down HA–Ub conjugates from HEK293T cell lysates expressing HA-tagged Ub. The asterisk denotes a cross-reactive band recognized by the HA-antibody. (**b**) The UBA domain is not required for cIAP2–MALT1 mediated polyubiquitylation of NEMO. The indicated cIAP2–MALT1 mutants were co-expressed with Strep-tagged-Ub and V5-tagged NEMO. Ubiquitylation of NEMO was determined by purifying Strep–Ub using Strep-Tactin-agarose resin and immunoblotting with an anti-V5 antibody. Note, Strep–Ub also immunoprecipitates non-ubiquitylated NEMO. This is due to the ability of NEMO to form homodimers, and, in this case, associates with ubiquitylated forms of NEMO. Levels of cIAP2–MALT1 and NEMO in lysates were determined using anti-FLAG and anti-V5 antibodies. (**c**) Self-oligomerization is normal in the cIAP2–MALT1$^{MF/AA}$ mutant but impaired in cIAP2–MALT1$^{\Delta BIR1}$. Oligomerization of cIAP2–MALT1 was determined by immunoprecipitation with anti-FLAG-agarose resin and immunoblotting with anti-V5. (**d**, **f**) cIAP2–MALT1 traps Lys 63-polyubiquitylated-NEMO. FLAG–cIAP2–MALT1 and FLAG–cIAP2–MALT1$^{MF/AA}$ immobilized on anti-FLAG-agarose resin were used to pull down unmodified NEMO and ubiquitylated forms of NEMO from HEK293T cellular lysates (**d**). cIAP2–MALT$^{MF/AA}$ fails to bind efficiently to polyubiquitylated NEMO. Note, in this assay (lane 8) cIAP2–MALT$^{MF/AA}$ also binds less efficiently to non-ubiquitylated NEMO. This is probably due to

the ability of NEMO to form homodimers whereby the non-modified form may have been co-purified through its association with polyubiquitylated NEMO. Mutation in the UBD of NEMO does not influence the binding of polyubiquitylated NEMO to cIAP2–MALT1. (**e**) cIAP2–MALT1 interacts with endogenous polyubiquitylated NEMO. The indicated constructs were expressed in HEK293T cells and binding to endogenous polyUb–NEMO was detected by immunoprecipitation with anti-FLAG–agarose resin and immunoblotting with anti-NEMO. (**g**) Model of cIAP2–MALT1-mediated NF-κB activation: the BIR1 domain of cIAP2 mediates oligomerization of cIAP2–MALT1 permitting recruitment of TRAF6 and unmodified NEMO, which weakly associates with cIAP2–MALT1. Following cIAP2–MALT1-assisted polyubiquitylation of NEMO, Lys 63-linked polyubiquitylated NEMO is tightly bound by cIAP2-MALT1 through UBA domain of cIAP2. This allows recruitment of TAK1, IKK activation and subsequent phosphorylation of IκBα, leading to its degradation and NF-κB-activation.